npj | climate and atmospheric science

Article

Published in partnership with CECCR at King Abdulaziz University

https://doi.org/10.1038/s41612-025-01285-5

No decrease of tropical convection in individual deep convective systems with global warming

Maximilien Bolot[1] ✉, Rémy Roca[2], Thomas Fiolleau[2] & Caroline Muller[3]

According to the scientific consensus, tropical convection must decrease with global warming. This decrease is manifested by a decrease of the mass transported in the upward branch of the atmospheric overturning circulation – the convective mass flux – and a connected decrease of high clouds in the tropics, with implications for climate sensitivity. By using kilometer-scale simulations in radiative-convective equilibrium and a convective tracking algorithm, we show that no such decrease occurs in storms when taken individually and that the mass transport per storm increases instead. Storms can achieve this result by aggregating more surface of the convective cores – the inner part of the storm doing the vertical transport – so that the decrease of tropical convection is actually explained by a decrease in the total number of storms. There is little variation of the mean pressure velocity in the cores of the storms, a robust finding of this study. This remarkable invariance of the mean pressure velocity points to an emerging property of convection that should receive more attention in future studies.

In the tropics, the atmosphere is heated from below by surface absorption of solar radiation and cooled from above by infrared emission to space at lower temperature[1]. This induces a thermally direct circulation, mediated by deep convection, which transports energy down the gradient of temperature while maintaining the mean temperature profile everywhere in the tropics close to a moist adiabat[2,3]. In the ascending branch of this circulation, deep convection transports mass and moisture upwards by converting potential energy of the positively buoyant air into kinetic energy of the convective motions[4,5]. In the descending branch, radiative cooling forces subsidence of the air. In statistical equilibrium over the tropics, the mass flux of the ascending branch, or convective mass flux, is equal to that of the descending branch, thereby creating an overturning circulation.

The overturning circulation in the tropics is expected to decrease under global warming[6–10]. Barring profound modifications in the physics of convection, this decrease must happen on grounds of energetics and has been discussed as such in the literature[11,12]. Namely, radiative cooling cannot keep up with the Clausius-Clapeyron increase of surface water vapor and effects thereof on upward energy transport, thus the convective mass flux must decrease to restore balance. This decrease has been shown in a hierarchy of models, from idealized simulations in radiative-convective equilibrium[13] to global climate models[9]. There is a sense in the literature that several changes with surface warming are connected to decreasing tropical convection. At large scale, reports of a weakening of the zonally-averaged Hadley circulation are consistent with a decrease of the convective mass flux in warmer conditions[14]. Moreover, a reduction in the bulk surface area of convective anvils, i.e. the extensive cirrus formations shielding the convective cores, has been interpreted as a manifestation of decreasing tropical convection as well[15,16]. This connection between decreases in surface area and in mass flux has been deemed important for its radiative implications, whereby a shrinking of convective surface with surface warming could allow more terrestrial radiation to escape to space, thus potentially producing a negative climate feedback[15,17–20].

The decrease of the convective mass flux can be simply understood from the energy budget in the descending branch of the overturning circulation, where downward advection of heat balances radiative cooling:

$$\left(\sum_i M_i\right) \times \frac{\partial s}{\partial T} = \frac{\partial F_{\mathrm{rad}}}{\partial T}\,, \tag{1}$$

where $\sum_i M_i$ is the convective mass flux (summed over individual convective storms $i = 1, 2, \ldots$), or equivalently the mass flux of the descending branch, F_{rad} is the net radiative flux, $s = c_p T + gz$ is dry static energy, with T temperature, z altitude, c_p specific heat capacity and g gravitational acceleration (Eq. (1) is adapted from previous work; see methods for derivation). Moisture effects have been discarded in Eq. (1) for the sake of simplicity but also modulate the energy constraint on mass flux[11] in the lower and middle troposphere (see methods). As mentioned above, the summation in the

[1]LMD/IPSL, CNRS, ENS-PSL, Ecole Polytechnique, Sorbonne Université, Paris, France. [2]LEGOS/OMP, CNES, CNRS, IRD, Université Toulouse III, Toulouse, France. [3]Institute of Science and Technology Austria (ISTA), Klosterneuburg, Austria. ✉e-mail: maximilien.bolot@lmd.ipsl.fr

mass flux indicates the contribution of individual storms to the total mass flux in the tropics. The term $\partial s/\partial T$, which represents a static stability, is equal to $g\left(1/\Gamma - 1/\Gamma_d\right)$, with Γ and Γ_d the tropical and dry adiabatic lapse rates, and increases with surface temperature as Γ departs from Γ_d. The radiative cooling $\partial F_{rad}/\partial T$ on the other hand is relatively independent of surface temperature when measured in temperature coordinate[21], as done in Eq. (1). Thus $\sum_i M_i$ must decrease with surface warming owing to strong energy constraints.

The goal of this paper is to show that, despite strong constraints on the bulk term, the mass fluxes M_i in individual storms need not decrease with surface warming, and may increase instead. The evolution of M_i is uncertain for a number of reasons. There is a sense that, in a warmer atmosphere, convection will be able to do more mechanical work and increase its production of kinetic energy[22,23]. The impact on mass flux is not clear however[24]. The uncertainty surrounding M_i is compounded by the fact that the many storm systems present in the tropics exhibit a variety of lifecycles, with an associated range of system durations and surface changes during the lifecycle[25]. The mass fluxes M_i are expected to vary during the lifecycle as well. Thus, the bulk constraint on mass fluxes need not transfer to individual systems. To show this, it is sufficient to exhibit a model where M_i increase with surface warming.

For this purpose, we use radiative-convective equilibrium (RCE) simulations of the System for Atmosphere Modeling (SAM)[26]. SAM uses anelastic momentum equations to resolve non-hydrostatic flows, thus allowing to explicitly resolve deep convection. The simulations are run in RCE long channel configuration (6144 × 384 km) at 3 km horizontal resolution and are integrated for 100 days, of which only the last 25 days are analyzed. Following the RCEMIP protocol[27], the simulations are run with surface temperatures of 300 K and 305 K. To identify and track in time the simulated tropical deep convective systems, hereafter referred to as DCSs[28,29], we use the Tracking Of Organized Convection Algorithm through a 3-D segmentatioN (TOOCAN)[30]. TOOCAN was originally designed to detect and track the tropical DCSs from infrared images acquired from a geostationary platform and has been adapted to run on the model output. The outer boundaries of the tracked DCSs are set by a 235 K brightness temperature (BT) threshold, which encompasses both the convective core of the DCSs – the inner part of the DCS doing the vertical transport – and the thick cirrus cloud shield immediately attached to it. (See methods and Supplementary Fig. S1).

Results

Decrease of mass flux and cloud coverage in aggregated statistics

Figure 1 shows the profiles of convective mass flux ($\sum_i M_i$, Fig. 1a) and cloud coverage (Fig. 1b) in temperature coordinate in the simulations. The convective mass flux – the vertical mass flux in the convective cores – has been computed by decomposing the vertical mass flux into bins of ice water path (IWP, the column-integrated ice water content). One can show from the time-mean overturning circulation in IWP coordinate that IWP is a good indicator of dynamic regime in the DCS (Supplementary Fig. S2)[31]. IWP > 1 kg m^{-2} marks the upward transport in the overturning circulation (with the bulk of updraft transport found above 5 kg m^{-2}) and is thus used as a criterion to select the convective cores. The cloud coverage is equal to the aggregated cloud coverage obtained with the DCS tracking algorithm.

We see that the convective mass flux decreases with surface warming at constant temperature in the atmosphere (Fig. 1a), illustrating the energy constraint formalized in Eq. (1). At the 250 K level, near the profile maximum, the decrease between the 300 K and 305 K simulations is about -20%. In the lower troposphere, below c.a. the 280 K level, the convective mass flux turns negative, but the change with surface warming still indicates a reduction of mass flux in absolute value. This turnover of mass flux indicates convective downdrafts and a cold-pool circulation at low levels organized by the latter (apparent in Supplementary Fig. S2). We note that the decrease of tropical convection may be measured through other means than the column-wise approach based on IWP and used in Fig. 1. For instance, one may take the maximum of the time-mean streamfunction in IWP and pressure coordinate as a measure of the total mass circulating in the overturning circulation (Supplementary Fig. S2). The reduction between the 300 K and 305 K simulations would be -21% in this case.

Connected to the decrease of convective mass flux is an observed decrease of cloud coverage with surface warming in the simulations (Fig. 1b). This decrease is traditionally explained by the decrease in convective mass flux (vertical) convergence which acts as a source of mass to the upper-level cirrus formations, as discussed for similar reported decreases in the scientific literature[15,32]. Note that the argument holds for thick cirrus formations directly attached to the convective cores, to which Fig. 1b relates, but not necessarily for thinner cirrus where unconstrained microphysical degrees of freedom may play a larger role and a link between convective mass flux and cloud surface area is not warranted[19].

We find that the results in Fig. 1 are independent of model resolution. This was checked from additional simulations of SAM run at 200 m horizontal resolution in a large-eddy simulation configuration (see methods). Similar decreases with surface warming of the convective mass flux and the cloud coverage were found with the higher-resolution configuration of the model (Supplementary Fig. S3).

Increase in individual systems

The convective mass flux $\sum_i M_i$ is made of many individual storm contributions M_i. Those storms, referred to as Deep Convective Systems (DCSs) in the scientific literature[33], are a manifestation of the fact that convection generally organizes at mesoscale in the tropics. The storms exhibit a lifecycle with an initiation, a growth and a dissipation stage, and propagate as they

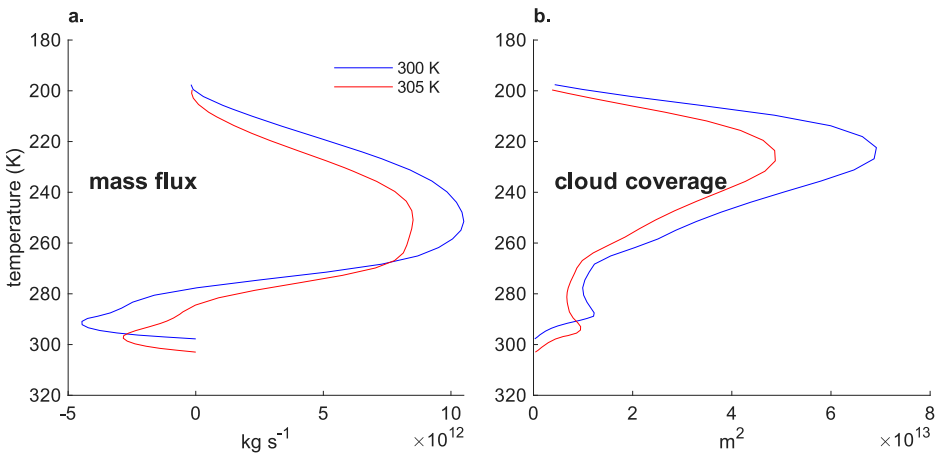

Fig. 1 | Convective mass flux and cloud coverage. Profiles in temperature coordinate of **a** the convective mass flux and **b** the cloud coverage in the simulations at 300 K (blue) and 305 K (red). The convective mass flux is computed over columns with IWP > 1 kg m^{-2}. Cloud is sampled over columns with BT < 235 K tracked by the TOOCAN algorithm. It encompasses convective core and anvil – the thick cirrus formations directly attached to the convective cores.

undergo this lifecycle. At any given time in the tropics, variance in properties such as M_i exists because (1) the storms are at different stages of their lifecycle and (2) the integrated strengths of those storms, as measured for instance by their total duration from the initiation to the dissipation stage, differ from each other.

Figure 2a shows the number of DCSs binned by DCS duration obtained by the tracking in time of those DCSs with the TOOCAN algorithm in the simulations at 300 K and 305 K. We find a strong decrease of the DCS number with surface warming. The total number shrinks from 4535 in the 300 K simulation to 2323 in the 305 K simulation, i.e. a 50% decrease. Figure 2a shows that the storms have a median lifetime of about 5 hours in both simulations. DCS occurrence decreases rapidly with increasing duration. (Note that the longer-lived DCSs also correspond on average to the "large" DCSs; see Fig. 2c). The long-lived (or "large") DCSs, in particular storms with lifetime above 10 hours, are disproportionately affected by surface warming as they disappear at a faster rate from the 305 K simulation than their shorter-lived counterparts. We see for instance (Supplementary Fig. S4) that the occurrence of storms with lifetimes of 6–8 h decreases by 50%, roughly in line with the mean, while that of storms with lifetime of 12–14 h decreases by 95%.

Long-lived DCSs carry a greater convective mass flux than their shorter-lived counterparts. This can be seen in Fig. 2b, which shows the mass flux per DCS in the 300 K and 305 K simulations, again binned by DCS duration. (The mass flux is computed on average over the duration of the DCS in each duration bin. The level of the maximum time-mean streamfunction in IWP and pressure coordinate is retained for computation. See Supplementary Fig. S2.) We see for instance that storms with lifetimes of 12–14 h carry 5 times the mass flux of those with lifetimes of 6–8 h. This means that the additional transport in long-lived DCSs is not just a result of larger lifetime but also results from additional mass flux per hour of DCS duration.

Figure 2b shows a dramatic increase with warming of the mass flux per individual DCS. The increase appears more pronounced in longer-lived DCSs but is observed at all durations. For instance, storms with a 6–8 h lifetime see an approximate doubling in mass flux from the 300 K to the 305 K simulation (blue vs red bars) and those with a 12–14 h lifetime see a nearly 4-fold increase. Thus, despite the constraint of a decrease with warming in the bulk statistics, the individual mass flux per system increases in these simulations.

Similar trends are seen in the surface area of the convective systems (Fig. 2c). Figure 2c shows the surface area per individual DCS of the convective cores and anvils (solid- and light-colored bars respectively). The transition from core to anvil, here set respectively to IWP > 1 kg m^{-2} and <1 kg m^{-2}, marks a transition from mostly vertical to mostly horizontal mass transport (Supplementary Fig. S2). We thus expect core surface area (i.e. where vertical transport occurs) to scale with convective mass flux, as confirmed in Fig. 2c. The increase in core surface area with system duration mirrors the trend in convective mass flux at constant climate (Fig. 2b). We also see that the anvils approximately maintain a fixed surface area ratio (~1.5) with the convective cores. The surface areas of the cores (and anvils) increase with warming (Fig. 2c, blue vs red bars). The increase appears to mirror that of the convective mass flux per individual system (Fig. 2b). The results thus suggest that the variance in convective mass flux in individual DCSs (whether at constant climate or the change with surface warming) is related to variance in core surface area in those systems.

Mass flux in individual systems follows surface area changes

The above discussion can be summarized by integrating the statistics over the distribution of lifetimes. That is, the bulk convective mass flux M can be simply written as

$$M = n\,d\,m\,, \tag{2}$$

where n is the number of DCSs, d the average DCS duration and m the average convective mass flux per individual DCS per hour of lifetime (note that comparing m among systems is equivalent to comparing the individual systems as if they lasted 1 h). Similarly, the surface area occupied by the convective cores C can be decomposed as

$$C = n\,d\,c\,, \tag{3}$$

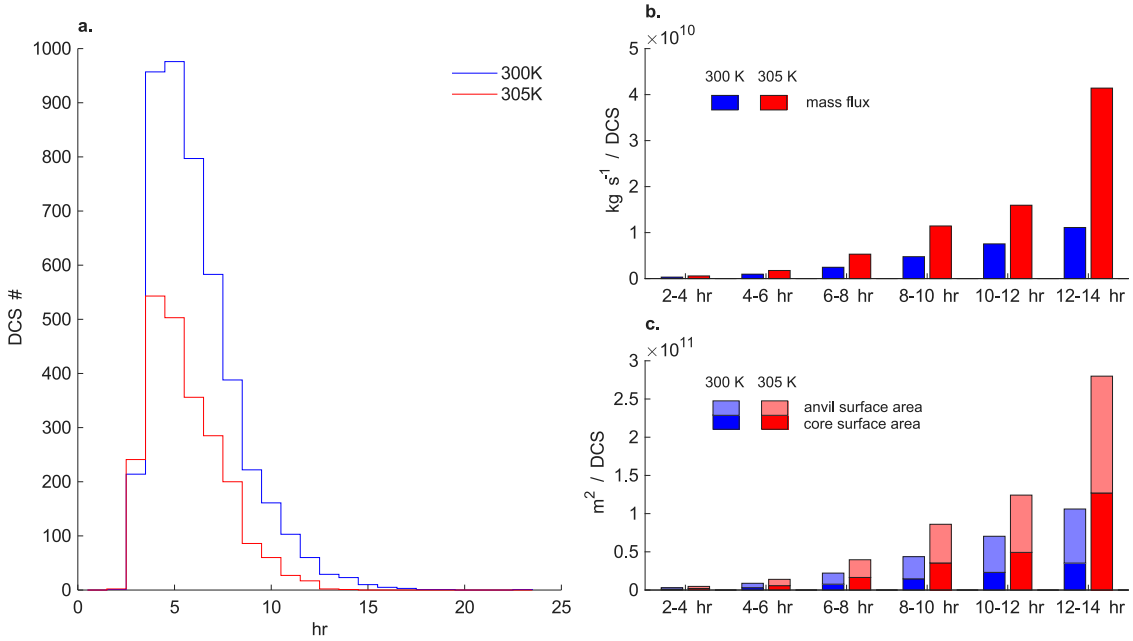

Fig. 2 | Convective mass flux and surface area evolution in individual systems. **a** Number of Deep Convective Systems (DCSs), **b** convective mass flux per DCS and **c** core and anvil surface area binned by DCS duration in the simulations at 300 K (blue) and 305 K (red). The convective mass flux is computed on average over the duration of the DCS in each duration bin at the vertical level of the maximum time-mean streamfunction in IWP and pressure coordinate (see Supplementary Fig. S2). The core and anvil surface areas are computed over columns with IWP > 1 kg m^{-2} and IWP < 1 kg m^{-2} within the tracked DCSs.

Table 1 | Summary of convective system properties in the simulations

Parameter	Symbol	300 K	305 K	% per K
DCS number	n	4535	2323	−13.4
DCS duration (hr)	d	5.6	5.1	−1.9
Anvil surface area (km^2)		5.1×10^7	3.2×10^7	−9.6
Anvil surface area per DCS (km^2/hr)		2.0×10^3	2.7×10^3	+5.7
Core surface area (km^2)	C	2.6×10^7	2.2×10^7	−3.3
Core surface area per DCS (km^2/hr)	c	1.0×10^3	1.9×10^3	+12.0
Mass flux[a] (kg s^{-1})	M	8.4×10^{12}	7.0×10^{12}	−3.4
Mass flux per DCS[a] (kg s^{-1}/hr)	m	3.3×10^8	5.9×10^8	+11.8
Mass flux density[a] (kg m^{-2} s^{-1})	m/c	0.32	0.32	−0.2
Mechanical work[a] (W)		5.1×10^{15}	8.1×10^{15}	+9.4
Mechanical work per DCS[a] (W hr^{-1})		2.0×10^{11}	6.8×10^{11}	+24.7
Mechanical work density[a] (W m^{-2})		193.6	364.4	+12.7
Ice[a] (kg)		1.2×10^{14}	1.2×10^{14}	+0.5
Ice per DCS[a] (kg hr^{-1})		4.5×10^9	9.9×10^9	+15.8
IWP[a] (kg m^{-2})		4.4	5.3	+3.8

The change with surface warming (last column) is computed using a geometric approach (see methods).
[a]Inside core only.

where c is the average core surface area per individual DCS per hour of lifetime. (Likewise, the decomposition can be applied to the anvil surface area, or any other quantity).

Results are presented in Table 1. The number of DCSs strongly decreases with surface warming, as previously noted in Fig. 2a, with a rate of decrease of −13.4% per 1-K surface temperature increase. The lifetime of the DCSs also slightly decreases with warming. The mass flux decreases by −3.4% K^{-1} in bulk statistics (M). This is reconciled by an increase of the mass flux in the individual systems of +11.8% K^{-1} (m). Thus, the global constraint on the convective mass flux is explained by the decreasing number of systems in those simulations. More precisely, the number of systems decreases faster than the mass flux per system increases as surface temperature increases. The core surface area evolution shows almost the exact same numbers: it decreases by −3.3% K^{-1} in bulk statistics (C) but increases by +12.0% K^{-1} per individual system (c).

This means that the convective mass flux density m/c (i.e., the convective mass flux per unit of core surface area) does not change significantly from the 300 K to the 305 K simulation. This number stays roughly invariant at 0.32 kg m^{-2} s^{-1} (Table 1). (It is also proportional to pressure velocity ω since $m/c = -\omega/g = \rho w$, with ρ the air density and w vertical velocity.) Thus, the increase in mass flux in individual systems is entirely accounted for by the increase in core surface area.

Discussion

Our results show that the decrease of the tropical overturning circulation in warmer conditions is explained by a decrease of core surface area in aggregated metrics. This decrease comes about through a decrease in the number of DCSs in a warmer atmosphere. This occurs despite an increase of individual DCS area. In other words, the number of DCSs decreases faster than the surface area per DCS increases. There is little effect from a change of the convective mass flux on average in the core (or equivalently from the mean pressure velocity in the core).

The pattern of fewer but larger systems with warming is reminiscent of published results on intensified self-aggregation[27]. More generally, the scientific literature may provide some clue on the mechanisms behind the decrease in system occurrence found in this study. On the one hand, there is a broad consensus that the area that can participate in convection is constrained to decrease with warming, as seen across multiple lines of evidence[34,35]. One argument in particular is connected to the increasing unevenness of sub-cloud moist static energy distribution with surface warming[35] (relevant in the context of RCE). On the other hand, arguments can be made that a warmer atmosphere may promote increased rates of convective generation, allowing the MCSs to grow to larger sizes[28]. Eventually, if larger systems compete for a smaller overall area, the occurrence of those systems must decrease. A detailed investigation of mechanisms behind the results of this paper is left to a future study.

The invariance of mean convective mass flux (or mean pressure velocity) in the core is remarkable and not obvious a priori. Indeed, the convective cores are expected to undergo significant changes as convection strengthens under surface warming[22,24,36]. We see for instance that the mechanical work performed in the cores increases from 194 W m^{-2} to 364 W m^{-2} in the simulation, i.e. by +12.7% K^{-1} (Table 1). As a result, vertical velocities increase inside the core. The invariance of the mean pressure velocity is explained in part by a compensating decrease in pressure as the updrafts move upward with rising isotherms in a warmer atmosphere. Other changes in the convective cores will alter the physics as well. For instance, the mean IWP in the cores increases by +3.8% K^{-1} (Table 1). This increase of ice loading in the cores forces convection to do more work to lift the water, thus impeding kinetic energy generation, which makes the invariance of the mean pressure velocity in the cores all the more remarkable as it results from many compensating factors.

Moreover, this result seems robust to the definition of the convective core used in the analysis. To show this, we replicate the analyses (see methods, Fig. S5) with the convective cores identified with the partitioning method of Marinescu et al.[37] – based on precipitation rates, vertical velocities and cloud mixing ratios instead of IWP. Under this new body of assumptions, the trend on mean pressure velocity in the cores remains negligible, at −0.8% K^{-1}, adding to the narrative of an invariance of pressure velocity in warmer conditions. It is also remarkable that this invariance of pressure velocity is observed across the whole distribution of DCS durations and not just in mean value (see Supplementary Fig. S6). That is, longer-lived (or "larger") systems have similar core pressure velocity as shorter-lived ("smaller") ones and this pressure velocity does not change with warming.

The invariance of pressure velocity, resulting from subtle compensations, means that variations in mass flux and variations in (core) surface area passively follow each other. In this perspective, the constrained decrease of the tropical convective mass flux is equivalent to a decrease in aggregate (core) surface area. The decrease (in mass flux or surface area) need not transfer to the scale of individual systems since the number of such systems is an unconstrained degree of freedom. More work is needed to check whether our results are reproducible with other models and tracking algorithms. More work is also needed to investigate how our results fit the existing theories of mass flux and anvil decrease with warming[11,12,15]. But our results show that the physics of the DCSs should receive more attention.

Large DCSs, in particular, may play a pivotal role in setting the mass flux distribution in the tropics. The largest systems, although few and far apart, are efficient enough[38] to set the vertical thermal structure of the tropics and thus, by considerations of energy balance, the overall convective mass flux (and core surface area) in aggregated metrics. This means that the largest DCSs would set the demand for vertical transport to be filled by the remainder of the DCS distribution. Ultimately, the physics of the DCSs will arbitrage between their number, lifetime and surface area evolution over their lifecycle.

Methods

Model and simulations

The System for Atmospheric Modeling (SAM version 6.11.2)[26] cloud-resolving model is used to produce long channel (6144 × 384 km) radiative-convective equilibrium simulations. The resolution is 3 km in both

horizontal directions, and the vertical resolution increases with height from a few tens of meters in the planetary boundary layer to 500 m in the mid and upper troposphere. The model uses the Rapid Radiative Transfer Model[39] for radiation, the MPDATA advection scheme, the default SAM1MOM one moment microphysical scheme and the TKE subgrid-scale closure (stationary Smagorinsky scheme, see Khairoutdinov and Randall[26] for details). The model solves the anelastic conservation equations for momentum, mass, energy and water, which is represented across six species (water vapor, cloud liquid, cloud ice, rain, snow and graupel). The upper third of the domain (18–27 km) has a sponge layer to absorb gravity waves, which would otherwise unrealistically fill our doubly-periodic domain.

The simulations in this study are following the RCEMIP protocol[40]. The integrations are performed as per the original protocol with a specific output frequency of 30 min instead of 1–3 h and the use of instantaneous fields instead of hourly averaged. The integration lasts 100 days and only the last 25 days are used and analyzed in this study to remove spin-up effects[27].

OLR to brightness temperature conversion

The tracking algorithm operates on a narrow band thermal infrared brightness temperature (BT) field akin to that of geostationary satellite meteorological observations. To apply the algorithm to model output, we first convert OLR into BT since the model outputs OLR. This is a typical procedure when applying cloud tracking algorithms to km-scale model simulations[41]. The procedure is modified though, to account for the idealized character of the simulations. BT5 (the BT of METEOSAT-5) is related to OLR via

$$\mathrm{OLR} = \sigma\, T_{\mathrm{Planck}}^4 \tag{4}$$

and

$$\mathrm{BT5} = a + b\, T_{\mathrm{Planck}} + c\, T_{\mathrm{Planck}}^2\,, \tag{5}$$

where σ is the Stephan-Boltzmann constant and a, b and c are fitting coefficients (with $a = -1022.66$, $b = 10.454$ and $c = -0.0216393$). These coefficients have been obtained by simulating the BT equivalent to that of METEOSAT-5 from the raw model thermodynamic and cloud outputs. The RTTOV forward radiative transfer (RTTOV-13)[42,43] is used for this purpose on 10 time steps (out of 1200) of the simulations. The Baran ice parametrization is used for ice clouds[44] along with the cumulus maritime option for water clouds. The coefficients of Eq. (5) are obtained by a linear regression between OLR and simulated BT5. This procedure yields a very small bias in the estimation of BT (1K) that does not impact the performance of the tracking nor alters the results of this study[45].

Identification of individual convective systems using TOOCAN

To identify and track deep convective systems, the Tracking Of Organized Convection Algorithm through a 3-D segmentatioN (TOOCAN) was applied on the SAM simulations with surface temperatures of 300 K and 305 K, following the methodology introduced by Fiolleau and Roca[30]. The core of TOOCAN is built on a spatio-temporal segmentation framework that operates in a three-dimensional domain (encompassing both space and time). Although originally developed for satellite observations, this framework was adapted for use with simulated convection fields without altering its fundamental principles.

The identification of DCSs begins with the detection of convective seeds within the three-dimensional brightness temperature (BT) field, using an initial threshold of 190 K. These cold seeds, when present, serve as starting points for a region-growing process driven by a 10-connected spatiotemporal operator. This operator gradually includes adjacent pixels with warmer BT values, expanding each detected seed up to a boundary that is 2 K warmer than its detection threshold. The region grows in an iterative manner: at each step, a new set of seeds is identified at a BT threshold 2 K warmer than the previous one, and each is expanded up to 2 K above its own detection threshold. For example, seeds detected at 192 K are grown to include neighboring pixels up to 194 K, and so on. This process continues until the final threshold of 235 K is reached, which marks the outer edge of the cold cloud shield typically associated with DCS cloud shields.

An important feature of the TOOCAN implementation for the RCE simulations was the use of a two-dimensional wrapping strategy to ensure continuity in DCS detection across the cyclic lateral boundaries of the SAM domain. In the zonal (X) direction, the final 1500 km of the domain, corresponding to 500 grid points, were duplicated and added to the beginning of each BT frame. Similarly, the first 1500 km were duplicated and added to the end of the frame. In the meridional (Y) direction, the entire BT field was duplicated and placed both above and below the original domain, extending it by 384 km on each side. This symmetrical domain extension ensures that convective systems crossing the domain boundaries are not fragmented or missed. After applying TOOCAN to the wrapped domain, all duplicate detections of the same DCS, caused by crossing boundaries, were systematically identified and either merged or removed during post-processing. This guarantees that no system is double-counted, preserving the physical integrity of each DCS's life cycle.

In total, 4535 DCSs were identified in the SAM simulation with a surface temperature of 300 K, while 2323 DCSs were detected in the SAM simulation conducted with a surface temperature of 305 K. This robust methodology allows for detailed characterization of each system throughout its entire life span within the full simulation domain. For each DCS, a suite of morphological properties was documented, including maximum area, lifetime duration, the evolution of the 90th percentile BT, cloud shield area, and other relevant metrics. These diagnostics form the basis for studying the organization, structure, and temporal evolution of convective activity in the simulated environment.

Convective mass flux from energy constraint

In the downward branch of the tropical overturning circulation, the downward advection of heat balances radiative and evaporative cooling. This can be written

$$gM\frac{\partial s}{\partial p} = Q_{\mathrm{rad}} - L\,e = g\frac{\partial F_{\mathrm{rad}}}{\partial p} - L\,e\,, \tag{6}$$

where M is the convective mass flux (units: kg m^{-2} s^{-1}), Q_{rad} is the radiative cooling rate (units: W kg^{-1}), F_{rad} is the net radiative flux (units: W m^{-2}), e is the evaporation rate (units: kg kg^{-1} s^{-1}), L is latent heat (units: J kg^{-1}), p is pressure (units: Pa), $s = c_pT + gz$ is dry static energy (units: J kg^{-1}), with T temperature (units: K), z altitude (units: m), c_p specific heat capacity (units: J K^{-1} kg^{-1}) and g gravitational acceleration (units: m s^{-2}). A full derivation of Eq. (6) (averaged at the tropical scale) from the local form of the energy continuity equation requires somewhat complex closures which may be found for instance in Yanai et al.[5] or Arakawa and Schubert[4]. For expediency, we can neglect the evaporation rate (a fairly reasonable approximation in the upper troposphere) and still get a sense of the energy constraint on M from Eq. (6). (Moisture effects modulate the constraint in the lower to middle troposphere. A derivation taking into account those effects may be found for instance in Jeevanjee[11].) Further multiplying by $\partial p/\partial T$ (as the isotherms are almost flat in the tropics), we can write the constraint in temperature coordinate:

$$M\frac{\partial s}{\partial T} = \frac{\partial F_{\mathrm{rad}}}{\partial T}\,. \tag{7}$$

Equation (7) is equivalent to Eq. (5) in Jeevanjee[11] with their coefficient α set to 1. (Note that M in Table 1 is area-integrated to yield the mass flux in the whole simulation domain; units: kg s^{-1}).

Sensitivity to the partitioning method used to identify the cores

Because the notion of convective core is central to this study (since vertical transport takes place in the cores), it is desirable to test the sensitivity of the results to the partitioning method used to identify the cores within the

tracked regions. We thus replicate the analyses of this study (Supplementary Table S1) with convective cores identified with the partitioning method of Marinescu et al.[37] – based upon precipitation rates, vertical velocities and cloud mixing ratios; see aforementioned reference – instead of our default partitioning using IWP > 1 kg m^{-2}. The histograms of IWP under both partitioning methods (Supplementary Fig. S4) show that the spatial selectivity differs between methods. The default partitioning shows of a weighting towards lower IWP with an abrupt cutoff at 1 kg m^{-2}, as prescribed by the method, encompassing a broader range of dynamic regimes in the core region. The Marinescu et al. partitioning exhibits a narrower dynamic range, biased towards stronger updrafts, with peak IWP weighting near 10 kg m^{-2}. It also produces narrower cores than the default method (2.7 times less surface area; 9.5×10^6 km^2 vs 2.6×10^7 km^2 in aggregated figures at 300 K; see Supplementary Table S1) and more extensive anvils accordingly (since anvils in this study are defined as the complement of the cores inside the domains BT < 235 K; see Supplementary Fig. S1). The mean mass flux density (or pressure velocity) in the core is roughly doubled over the default method value (0.6 kg m^{-2} s^{-1} vs 0.3 kg m^{-2} s^{-1}), consistent with a stronger updraft bias. We do see, however, that the trend with surface warming of pressure velocity in these narrower cores identified under the alternate partitioning stays negligible (−0.8% K^{-1} vs −0.2% K^{-1} for the default method value).

Tendencies with warming

The variation (in percent) of a variable x between the simulations at 300 K and 305 K is computed using a geometric approach:

$$\%x = \frac{100}{\Delta T}\log\left(\frac{x_2}{x_1}\right), \tag{8}$$

where x_1 and x_2 are the states of x at 300 K and 305 K and $\Delta T = 5\,K$. Application of the above formula ensures that the variation of $x = x_1x_2x_3...$ is equal to $\%x = \%x_1 + \%x_2 + \%x_3 + ...$ with no need for consideration of a non-linear term. For small variations of x, this approach yields similar results to an approach based on finite differences.

Mechanical work

The mechanical work W done by the DCS is computed following Pauluis[22]:

$$W = \int_\Omega \overline{\rho} g w \left(\frac{T - \overline{T}}{\overline{T}} + \frac{R_v}{R_d} q_v\right), \tag{9}$$

where ρ is density, w vertical velocity, T temperature, q_v water vapor mixing ratio and g, R_v, R_d are the gravitational acceleration and the moist and dry gas constants respectively. $\overline{\rho}$ and $\overline{T}$ are the horizontally averaged density and temperature (i.e. the reference state in the anelastic framework). $\int_\Omega = \int dx\,dy\,dz$ denotes the integral over an entire atmospheric domain (in the case of W in Table 1, this is the aggregate core volume).

Data availability

SAM is available at http://rossby.msrc.sunysb.edu/SAM/, accessed on Jun 29 2025. The convective tracking dataset used in this study – SAM RCE simulations tracked by the TOOCAN algorithm – is available at https://doi.org/10.14768/d8556f23-9ba6-4c31-a134-21ef0b4e948e.

Code availability

Codes and data to reproduce the figures of this paper are available at https://doi.org/10.5281/zenodo.15766829.

Received: 21 July 2025; Accepted: 27 November 2025;
Published online: 12 December 2025

References

1. Emanuel, K. A., David Neelin, J. & Bretherton, C. S. On large-scale circulations in convecting atmospheres. *Q. J. R. Meteorological Soc.* **120**, 1111–1143 (1994).
2. Pierrehumbert, R. T. Thermostats, radiator fins, and the local runaway greenhouse. *J. Atmos. Sci.* **52**, 1784–1806 (1995).
3. Sobel, A. H. & Bretherton, C. S. Modeling tropical precipitation in a single column. *J. Clim.* **13**, 4378–4392 (2000).
4. Arakawa, A. & Schubert, W. H. Interaction of a Cumulus Cloud Ensemble with the Large-Scale Environment, Part I. *J. Atmos. Sci.* **31**, 674–701 (1974).
5. Yanai, M., Esbensen, S. & Chu, J.-H. Determination of Bulk Properties of Tropical Cloud Clusters from Large-Scale Heat and Moisture Budgets. *J. Atmos. Sci.* **30**, 611–627 (1973).
6. Betts, A. K. & Ridgway, W. Climatic equilibrium of the atmospheric convective boundary layer over a tropical ocean. *J. Atmos. Sci.* **46**, 2621–2641 (1989).
7. Held, I. M. & Soden, B. J. Robust Responses of the Hydrological Cycle to Global Warming. *J. Clim.* **19**, 5686–5699 (2006).
8. Larson, K., Hartmann, D. L. & Klein, S. A. The role of clouds, water vapor, circulation, and boundary layer structure in the sensitivity of the tropical climate. *J. Clim.* **12**, 2359–2374 (1999).
9. Vecchi, G. A. & Soden, B. J. Global warming and the weakening of the tropical circulation. *J. Clim.* **20**, 4316–4340 (2007).
10. Jenney, A. M., Randall, D. A. & Branson, M. D. Understanding the response of tropical ascent to warming using an energy balance framework. *J. Adv. Model. Earth Syst.* **12**, e2020MS002056 (2020).
11. Jeevanjee, N. Three rules for the decrease of tropical convection with global warming. *J. Adv. Model. Earth Syst.* **14**, e2022MS003285 (2022).
12. Williams, A. I. L. & Jeevanjee, N. A robust constraint on the response of convective mass fluxes to warming. *J. Adv. Model. Earth Syst.* **17**, e2024MS004695 (2025).
13. Silvers, L. G., Reed, K. A. & Wing, A. A. The response of the large-scale tropical circulation to warming. *J. Adv. Model. Earth Syst.* **15**, e2021MS002966 (2023).
14. Merlis, T. M. & Schneider, T. Changes in zonal surface temperature gradients and walker circulations in a wide range of climates. *J. Clim.* **24**, 4757–4768 (2011).
15. Bony, S. et al. Thermodynamic control of anvil cloud amount. *Proc. Natl. Acad. Sci.* **113**, 8927–8932 (2016).
16. Su, H. et al. Tightening of tropical ascent and high clouds key to precipitation change in a warmer climate. *Nat. Commun.* **8**, 15771 (2017).
17. Sherwood, S. C. et al. An assessment of Earth's climate sensitivity using multiple lines of evidence. *Rev. Geophys.* **58**, e2019RG000678 (2020).
18. Gasparini, B. et al. Opinion: tropical cirrus – from micro-scale processes to climate-scale impacts. *Atmos. Chem. Phys.* **23**, 15413–15444 (2023).
19. Sokol, A. B., Wall, C. J. & Hartmann, D. L. Greater climate sensitivity implied by anvil cloud thinning. *Nat. Geosci.* **17**, 398–403 (2024).
20. McKim, B., Bony, S. & Dufresne, J.-L. Weak anvil cloud area feedback suggested by physical and observational constraints. *Nat. Geosci.* **17**, 392–397 (2024).
21. Jeevanjee, N. & Romps, D. M. Mean precipitation change from a deepening troposphere. *Proc. Natl. Acad. Sci.* **115**, 11465–11470 (2018).
22. Pauluis, O. & Held, I. M. Entropy budget of an atmosphere in radiative–convective equilibrium. Part I: maximum work and frictional dissipation. *J. Atmos. Sci.* **59**, 125–139 (2002).
23. Singh, M. S. & O'Gorman, P. A. Increases in moist-convective updraught velocities with warming in radiative-convective equilibrium. *Q. J. R. Meteorol. Soc.* **141**, 2828–2838 (2015).
24. Muller, C. & Takayabu, Y. Response of precipitation extremes to warming: What have we learned from theory and idealized cloud-resolving simulations, and what remains to be learned?. *Environ. Res. Lett.* **15**, 035001 (2020).

25. Roca, R. & Fiolleau, T. Extreme precipitation in the tropics is closely associated with long-lived convective systems. *Commun. Earth Environ.* **1**, 1–6 (2020).
26. Khairoutdinov, M. F. & Randall, D. A. Cloud resolving modeling of the ARM Summer 1997 IOP: model formulation, results, uncertainties, and sensitivities. *J. Atmos. Sci.* **60**, 607–625 (2003).
27. Wing, A. A. et al. Clouds and convective self-aggregation in a multimodel ensemble of radiative-convective equilibrium simulations. *J. Adv. Model. Earth Syst.* **12**, e2020MS002138 (2020).
28. Houze, R. A. Mesoscale convective systems. *Rev. Geophys.* **42**, 1–43 (2004).
29. Feng, Z. et al. Mesoscale convective systems in DYAMOND global convection-permitting simulations. *Geophys. Res. Lett.* **50**, e2022GL102603 (2023).
30. Fiolleau, T. & Roca, R. An algorithm for the detection and tracking of tropical mesoscale convective systems using infrared images from geostationary satellite. *IEEE Trans. Geosci. Remote Sens.* **51**, 4302–4315 (2013).
31. Bolot, M. et al. Kilometer-scale global warming simulations and active sensors reveal changes in tropical deep convection. *npj Clim. Atmos. Sci.* **6**, 1–8 (2023).
32. Seeley, J. T., Jeevanjee, N., Langhans, W. & Romps, D. M. Formation of tropical anvil clouds by slow evaporation. *Geophys. Res. Lett.* **46**, 492–501 (2019).
33. Roca, R., Fiolleau, T. & Netz, L. Scale-dependence of tropical oceanic deep convective systems' cloud shield morphology to environmental conditions. *J. Geophys. Res. Atmos.* **130**, e2024JD042494 (2025).
34. Chou, C. & Neelin, J. D. Mechanisms of global warming impacts on regional tropical precipitation. *J. Clim.* **17**, 2688–2701 (2004).
35. Zhang, Y. & Fueglistaler, S. Mechanism for increasing tropical rainfall unevenness with global warming. *Geophys. Res. Lett.* **46**, 14836–14843 (2019).
36. Romps, D. M. Clausius–Clapeyron scaling of CAPE from analytical solutions to RCE. *J. Atmos. Sci.* **73**, 3719–3737 (2016).
37. Marinescu, P. J., van den Heever, S. C., Saleeby, S. M. & Kreidenweis, S. M. The microphysical contributions to and evolution of latent heating profiles in two MC3E MCSs. *J. Geophys. Res. Atmos.* **121**, 7913–7935 (2016).
38. Li, Y.-X., Masunaga, H., Takahashi, H. & Yu, J.-Y. When, where and to what extent do temperature perturbations near tropical deep convection follow convective quasi equilibrium?. *Geophys. Res. Lett.* **51**, e2024GL108233 (2024).
39. Mlawer, E. J., Taubman, S. J., Brown, P. D., Iacono, M. J. & Clough, S. A. Radiative transfer for inhomogeneous atmospheres: RRTM, a validated correlated-k model for the longwave. *J. Geophys. Res. Atmos.* **102**, 16663–16682 (1997).
40. Wing, A. A. et al. Radiative–convective equilibrium model intercomparison project. *Geosci. Model Dev.* **11**, 793–813 (2018).
41. Feng, Z. et al. Mesoscale convective systems tracking method intercomparison (MCSMIP): application to DYAMOND global km-scale simulations. *J. Geophys. Res. Atmos.* **130**, e2024JD042204 (2025).
42. Saunders, R. et al. An update on the RTTOV fast radiative transfer model (currently at version 12). *Geosci. Model Dev.* **11**, 2717–2737 (2018).
43. Geer, A. J. et al. Bulk hydrometeor optical properties for microwave and sub-millimetre radiative transfer in RTTOV-SCATT v13.0. *Geosci. Model Dev.* **14**, 7497–7526 (2021).
44. Vidot, J., Baran, A. J. & Brunel, P. A new ice cloud parameterization for infrared radiative transfer simulation of cloudy radiances: evaluation and optimization with IIR observations and ice cloud profile retrieval products. *J. Geophys. Res. Atmos.* **120**, 6937–6951 (2015).
45. Fiolleau, T. & Roca, R. A database of deep convective systems derived from the intercalibrated meteorological geostationary satellite fleet and the TOOCAN algorithm (2012–2020). *Earth Syst. Sci. Data* **16**, 4021–4050 (2024).

Acknowledgements

We thank Sophie Cloché for her support with the handling of the various datasets. This study benefited from the IPSL mesocenter ESPRI facility which is supported by CNRS, UPMC, Labex L-IPSL, CNES and Ecole Polytechnique. The authors acknowledge the CNES and CNRS support under the Megha-Tropiques program. C.M. gratefully acknowledges funding from the European Research Council (ERC) under the European Union's Horizon 2020 research and innovation program (Project CLUSTER, Grant Agreement No. 805041).

Author contributions

M.B. and R.R. designed the research. C.M. performed the simulations. T.F. performed the convective tracking activities. All authors wrote the paper.

Competing interests

The authors declare no competing interests.

Additional information

Supplementary information The online version contains supplementary material available at https://doi.org/10.1038/s41612-025-01285-5.

Correspondence and requests for materials should be addressed to Maximilien Bolot.